Scattering by FSS on Anisotropic Substrate for TE and TM Excitation

Antonio Luiz P. S. Campos, *Student Member, IEEE*, Adaildo Gomes d'Assunção, *Member, IEEE*, and Laércio Martins de Mendonça

***Abstract*—The scattering of electromagnetic waves from frequency-selective surfaces (FSS) composed of rectangular conducting patches mounted on uniaxial dielectric anisotropic substrate is investigated by using a full-wave analysis. The moment method is used in combination with the spectral-domain immitance approach to determine reflection and transmission coefficients of the FSS structure as function of the geometry parameters and dielectric anisotropy. The analysis provides very accurate results compared to those presented by others and to those obtained by measurements.**

***Index Terms*—Anisotropic substrate, dielectric anisotropy, frequency-selective surfaces, FSS.**

I. Introduction

FREQUENCY-SELECTIVE surfaces (FSS), with conducting patches or apertures in conducting screens, are used in the development of several microwave integrated circuits and antennas [1]–[6]. For instance, microwave multiband antennas were developed by depositing conducting patches on a dielectric substrate [6]. Furthermore, some recent works were reported on FSS structures with magnetized ferrimagnetic substrates [3], with liquid substrates, and integrated with active devices [4], [5].

The aim of this paper is to investigate the effect produced by anisotropic dielectric substrates in the scattering characteristics of incident electromagnetic waves on FSS structures, such as those shown in Fig. 1.

The analysis is performed in the Fourier domain. The electromagnetic scattering problem is formulated and the spectral-domain immitance approach is used to determine the components for the structure Green's function. The knowledge of these components allows, with the use of the moment method, to obtain the reflection and transmission characteristics of the analyzed structure.

For purposes of comparison, numerical results were calculated for the reflection coefficient versus frequency, for freestanding FSS. Furthermore, numerical results were obtained for the transmission coefficient through an FSS on a dielectric layer in order to be compared with experimental results. A very good agreement was observed between our results and those presented by others [7] for several particular cases. Also, our numerical results are in good agreement with the measured data.

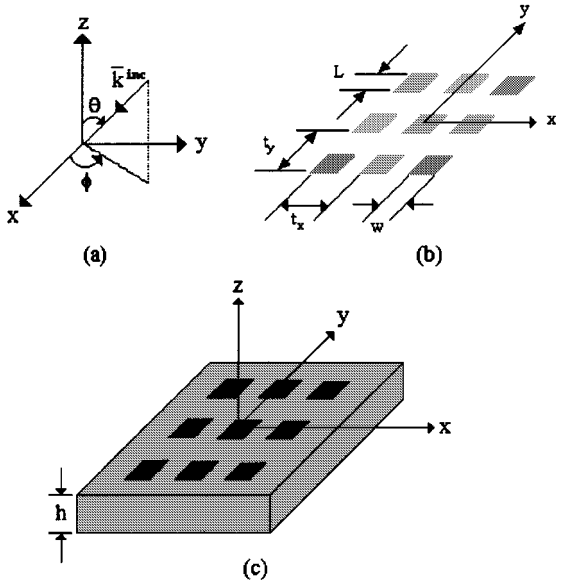

Fig. 1. FSS structures. (a) Incident plane wave. (b) Freestanding FSS. (c) FSS on uniaxial anisotropic dielectric substrate.

II. Formulation of the FSS Scattering Problem

The structure considered in this paper is shown in Fig. 1(c). The basic structure is made of periodic rectangular conducting patches, with very small thickness, mounted on an uniaxial anisotropic dielectric layer [8].

The dielectric substrate permittivity tensor is [6]

$$\bar{\bar{\epsilon}} = \epsilon_0 \begin{bmatrix} \epsilon_{xx} & 0 & 0 \\ 0 & \epsilon_{xx} & 0 \\ 0 & 0 & \epsilon_{zz} \end{bmatrix} \tag{1}$$

where ϵ_{xx} and ϵ_{zz} are the components of the relative electric permittivity along the x- and z-directions, respectively, and ϵ_0 is the free-space electric permittivity. Furthermore, the optical axis in the substrate layer is oriented along the z-direction, which is perpendicular to the plane of the conducting patches [see Fig. 1(c)].

In this paper, the spectral-domain immitance approach is used to obtain the dyadic Green's function [9]. The moment method is then used to determine the reflection and transmission characteristics for the FSS structures (Fig. 1).

Manuscript received March 30, 2000; revised July 26, 2001.

A. L. P. S. Campos is with the Department of Electrical Engineering, Federal University of Paraíba, 58109-970, Campina Grande PB, Brazil (e-mail: alcampos@dee.ufpb.br).

A. G. d'Assunção and L. M. de Mendonça are with the Department of Electrical Engineering, Federal University of Rio Grande do Norte, 59072-970 Natal RN, Brazil (e-mail: adaildo@ct.ufrn.br).

Publisher Item Identifier S 0018-9480(02)00754-8.

The first step in the formulation of the electromagnetic scattering problem on an FSS is to relate the scattered fields and the surface-induced currents on the conducting patches due to the incident field. To accomplish that, the operator equation of the electric field is derived for a freestanding FSS structure [see Fig. 1(b)], considering perfectly electric conducting rectangular patches. The derivation is then extended to analyze FSS structures on uniaxial anisotropic dielectric layers, such as the one shown in Fig. 1(c) [6].

The scattered field from the conducting patches in the plane x–y (Fig. 1) due to incident plane wave can be calculated from the surface-induced current on the patch. Thus, the scattered field is given by [2]

$$E^S = -j\omega\mu_0\vec{A} + \frac{1}{j\omega\epsilon_0}\nabla\left(\nabla\cdot\vec{A}\right) \tag{2}$$

where μ_0 and ϵ_0 are the free-space magnetic permeability and electric permittivity, respectively. In (2), $\vec{A}$ is the magnetic potential vector, which is given by

$$\vec{A} = \overline{\overline{Z}} * \vec{J}. \tag{3}$$

The asterisk in (3) means the convolution operation, $\vec{J}$ is the surface-induced current in the conducting patch, and $\overline{\overline{Z}}$ is the dyadic Green's function in free space. Considering that the patch is made of a perfectly electric conducting material, the tangential electric field, denoted by the subscript t, is given by

$$\vec{E}_t = \vec{E}_t^S + \vec{E}_t^{\text{inc}} = 0. \tag{4}$$

The superscripts $\overline{s}$ and $\overline{\text{inc}}$ in (4) refer to the scattered and incident fields, respectively. Consequently, from (2), the incident field is expressed as

$$E^{\text{inc}} = j\omega\mu_0\vec{A} - \frac{1}{j\omega\epsilon_0}\nabla\left(\nabla\cdot\vec{A}\right). \tag{5}$$

For a planar surface with a very small thickness, only the surface current density components J_x and J_y exist and, as a consequence, only A_x and A_y have nonzero values. Thus, (5) is rewritten in a matrix form as

$$-\begin{bmatrix} E_x^{\text{inc}} \\ E_y^{\text{inc}} \end{bmatrix} = \frac{1}{j\omega\epsilon_0}\begin{bmatrix} \dfrac{\partial^2}{\partial x^2}+k_0^2 & \dfrac{\partial^2}{\partial x\partial y} \\ \dfrac{\partial^2}{\partial x\partial y} & \dfrac{\partial^2}{\partial y^2}+k_0^2 \end{bmatrix}\begin{bmatrix} A_x \\ A_y \end{bmatrix} \tag{6}$$

with $A_x = \overline{\overline{Z}} * J_x$ and $A_y = \overline{\overline{Z}} * J_y$, according to (3).

Furthermore, by applying the Fourier transform in (6), one obtains

$$-\begin{bmatrix} \tilde{E}_x^{\text{inc}} \\ \tilde{E}_y^{\text{inc}} \end{bmatrix} = \frac{1}{j\omega\epsilon_0}\begin{bmatrix} k_0^2-\alpha^2 & -\alpha\beta \\ -\alpha\beta & k_0^2-\beta^2 \end{bmatrix}\left[\tilde{Z}\right]\begin{bmatrix} \tilde{J}_x \\ \tilde{J}_y \end{bmatrix}. \tag{7}$$

Using the inverse Fourier transform, (7) is rewritten as

$$-\begin{bmatrix} E_x^{\text{inc}} \\ E_y^{\text{inc}} \end{bmatrix} = \frac{1}{(2\pi)^2}\sum_{-\infty}^{\infty}\sum_{-\infty}^{\infty}\frac{1}{j\omega\epsilon_0}\begin{bmatrix} k_0^2-\alpha^2 & -\alpha\beta \\ -\alpha\beta & k_0^2-\beta^2 \end{bmatrix} \cdot\left[\tilde{Z}\right]\begin{bmatrix} \tilde{J}_x \\ \tilde{J}_y \end{bmatrix}e^{j(\alpha x+\beta y)}d\alpha d\beta. \tag{8}$$

To extend this formulation to analyze a periodic array of patches on a dielectric substrate, the characteristic equation, given in (8), is modified, by substituting the dyadic Green's function by a new one for the periodic structure. Therefore, (8) is rewritten as

$$-\begin{bmatrix} E_x^{\text{inc}} \\ E_y^{\text{inc}} \end{bmatrix} = \sum_{m=-\infty}^{\infty}\sum_{n=-\infty}^{\infty}\begin{bmatrix} \tilde{Z}_{xx} & \tilde{Z}_{xy} \\ \tilde{Z}_{yx} & \tilde{Z}_{yy} \end{bmatrix}\begin{bmatrix} \tilde{J}_x(\alpha_m,\beta_n) \\ \tilde{J}_y(\alpha_m,\beta_n) \end{bmatrix}e^{j(\alpha_m x+\beta_n y)} \tag{9}$$

where E_x^{inc} and E_x^{inc} are the incident electric-field components along the x- and y-directions, respectively. In (9), $\tilde{Z}_{xx}$, $\tilde{Z}_{xy}$, $\tilde{Z}_{yx}$, and $\tilde{Z}_{yy}$ are the components of the Green's function, while $\tilde{J}_x$ and $\tilde{J}_y$ are the Fourier-transformed current density components along the x- and y-directions, respectively. The spectral variables α_m and β_n are given by

$$\alpha_m = \frac{2\pi m}{t_x} + k_0\sin(\theta)\cos(\phi) \tag{10}$$

$$\beta_n = \frac{2\pi n}{t_y} + k_0\sin(\theta)\sin(\phi) \tag{11}$$

where t_x and t_y are the periods of the cells in the x- and y-directions, respectively. The incidence angles are θ and ϕ [see Fig. 1(a)].

The dyadic Green's function components are determined as

$$\tilde{Z}_{xx} = \frac{1}{\alpha_m^2+\beta_n^2}\left(\beta_n^2\tilde{Z}^{\text{TM}} + \alpha_m^2\tilde{Z}^{\text{TE}}\right) \tag{12}$$

$$\tilde{Z}_{xy} = \tilde{Z}_{yx} = \frac{\alpha_m\beta_n}{\alpha_m^2+\beta_n^2}\left(\tilde{Z}^{\text{TE}} - \tilde{Z}^{\text{TM}}\right) \tag{13}$$

$$\tilde{Z}_{yy} = \frac{1}{\alpha_m^2+\beta_n^2}\left(\beta_n^2\tilde{Z}^{\text{TE}} + \alpha_m^2\tilde{Z}^{\text{TM}}\right) \tag{14}$$

where [8]

$$\tilde{Z}^{TM,TE} = \frac{1}{Y_+^{e,h}+Y_-^{e,h}}. \tag{15}$$

For the uniaxial anisotropic case with an optical axis in the z-direction (Fig. 1), we define

$$Y_{0i}^{\text{TE}} = \frac{\gamma_{hi}}{j\omega\mu_0} \tag{16}$$

$$Y_{0i}^{\text{TM}} = \frac{j\omega\epsilon_0\epsilon_{xxi}}{\gamma_{ei}} \tag{17}$$

$$\gamma_{ei} = \sqrt{\frac{\epsilon_{xxi}}{\epsilon_{zzi}}\left(\alpha_m^2+\beta_n^2-\omega^2\mu_0\epsilon_0-\epsilon_{zzi}\right)} \tag{18}$$

$$\gamma_{hi} = \sqrt{\alpha_m^2+\beta_n^2-\omega^2\mu_0\epsilon_0-\epsilon_{xxi}} \tag{19}$$

and γ_0 is obtained by considering $\epsilon_{xx} = \epsilon_{zz} = 1$.

The impedances $\tilde{Z}^{\text{TM}}$ and $\tilde{Z}^{\text{TM}}$ in (15) are given by

$$\tilde{Z}^{\text{TM}} = \frac{\gamma_0\gamma_e\left[\gamma_e+\epsilon_{xx}\gamma_0\coth(\gamma_e h)\right]}{j\omega\epsilon_0\left[\gamma_e^2+2\epsilon_{xx}\gamma_0\gamma_e\coth(\gamma_e h)+\gamma_0^2\epsilon_{xx}^2\right]} \tag{20}$$

$$\tilde{Z}^{\text{TE}} = \frac{j\omega\mu_0\left[\gamma_0+\gamma_h\coth(\gamma_h h)\right]}{\gamma_h^2+2\gamma_0\gamma_h\coth(\gamma_h h)+\gamma_0^2}. \tag{21}$$

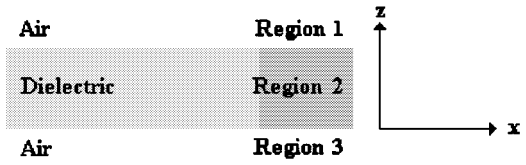

Fig. 2. FSS dielectric layers considered in the derivation of the incident field expressions.

The transverse components of the incident field on the conducting surfaces are derived by using the z-directed potential vector in each of the dielectric layered regions, shown in Fig. 2.

Enforcing the appropriate continuity conditions at each dielectric interface (Fig. 2), two expressions for the incident fields on the conducting surfaces are obtained as follows.

For TE modes:

$$\begin{bmatrix} E_x^{\text{inc}} \\ E_y^{\text{inc}} \end{bmatrix} = 2j\gamma_0 \frac{\gamma_0 + \gamma_h \coth(\gamma_h h)}{\gamma_h^2 + 2\gamma_0\gamma_h \coth(\gamma_h h) + \gamma_0^2} e^{j(\alpha_0 x + \beta_0 y)} \begin{bmatrix} -\beta_0 \\ \alpha_0 \end{bmatrix}. \tag{22}$$

For TM modes:

$$\begin{bmatrix} E_x^{\text{inc}} \\ E_y^{\text{inc}} \end{bmatrix} = \frac{2\gamma_0\gamma_e}{\omega\epsilon_0} \frac{\gamma_e + \gamma_0\epsilon_{xx} \coth(\gamma_e h)}{\gamma_e^2 + 2\epsilon_{xx}\gamma_0\gamma_e \coth(\gamma_e h) + \gamma_0^2\epsilon_{xx}} e^{j(\alpha_0 x + \beta_0 y)} \begin{bmatrix} \alpha_0 \\ \beta_0 \end{bmatrix}. \tag{23}$$

We then substituted the expressions for the incident fields and dyadic Green's function in the operator equation for the induced current density shown in (9). Finally, this equation is solved for the FSS structure on a anisotropic dielectric substrate.

The reflection and transmission coefficients are given by [2]

$$R_{mn}^{\text{TE}} = \frac{j}{\alpha_m^2 + \beta_n^2} \left\{ \beta_n \left(\tilde{E}_{xt}^s(\alpha_m, \beta_n) + \tilde{E}_x^r \delta_{mn} \right) - \alpha_m \left(\tilde{E}_{yt}^s(\alpha_m, \beta_n) + \tilde{E}_y^r \delta_{mn} \right) \right\} \tag{24}$$

$$R_{mn}^{\text{TM}} = \frac{-1}{(\alpha_m^2 + \beta_n^2)\frac{\gamma_{mn}}{\omega\epsilon_0}} \left\{ \alpha_m \left(\tilde{E}_{xt}^s(\alpha_m, \beta_n) + \tilde{E}_x^r \delta_{mn} \right) - \beta_n \left(\tilde{E}_{yt}^s(\alpha_m, \beta_n) + \tilde{E}_y^r \delta_{mn} \right) \right\} \tag{25}$$

$$T_{mn}^{\text{TE}} = \frac{j}{\alpha_m^2 + \beta_n^2} \left\{ \beta_n \left(\tilde{E}_{xb}^s(\alpha_m, \beta_n) + \tilde{E}_x^t \delta_{mn} \right) - \alpha_m \left(\tilde{E}_{yb}^s(\alpha_m, \beta_n) + \tilde{E}_y^t \delta_{mn} \right) \right\} \tag{26}$$

$$T_{mn}^{\text{TM}} = \frac{-1}{(\alpha_m^2 + \beta_n^2)\frac{\gamma_{mn}}{\omega\epsilon_0}} \left\{ \alpha_m \left(\tilde{E}_{xb}^s(\alpha_m, \beta_n) + \tilde{E}_x^t \delta_{mn} \right) - \beta_n \left(\tilde{E}_{yb}^s(\alpha_m, \beta_n) + \tilde{E}_y^t \delta_{mn} \right) \right\} \tag{27}$$

where γ_{mn} and δ_{mn} are, respectively, the propagation constant and Kronecker delta.

The scattered fields in the top (t) and bottom (b) regions of the structure (Fig. 2) due to incident fields on the conducting surfaces are given by

$$-\begin{bmatrix} \tilde{E}_{xt,b}^s \\ \tilde{E}_{yt,b}^s \end{bmatrix} = \begin{bmatrix} \tilde{Z}_{xxt,b} & \tilde{Z}_{xyt,b} \\ \tilde{Z}_{yxt,b} & \tilde{Z}_{yyt,b} \end{bmatrix} \begin{bmatrix} \tilde{J}_x \\ \tilde{J}_y \end{bmatrix} \tag{28}$$

where the components of the Green's function in the top of the structure are given by (12)–(14).

The components of the Green's function in the bottom region of this structure are given by

$$\tilde{Z}_{xxb} = \frac{1}{\alpha_m^2 + \beta_n^2} \left(\beta_n^2 \tilde{Z}_b^{\text{TM}} + \alpha_m^2 \tilde{Z}_b^{\text{TE}} \right) \tag{29}$$

$$\tilde{Z}_{xyb} = \tilde{Z}_{yxb} = \frac{\alpha_m \beta_n}{\alpha_m^2 + \beta_n^2} \left(\tilde{Z}_b^{\text{TE}} - \tilde{Z}_b^{\text{TM}} \right) \tag{30}$$

$$\tilde{Z}_{yyb} = \frac{1}{\alpha_m^2 + \beta_n^2} \left(\beta_n^2 \tilde{Z}_b^{\text{TE}} + \alpha_m^2 \tilde{Z}_b^{\text{TM}} \right) \tag{31}$$

where

$$\tilde{Z}_b^{TM,TE} = \frac{1}{Y_+^{e,h} + Y_-^{e,h}} Y_{\text{Transf.}}^{e,h} \tag{32}$$

and

$$Y_{\text{Transf.}}^{e} = \frac{\gamma_0\epsilon_{xx}}{\gamma_0\epsilon_{xx} \cosh(\gamma_e h) + \gamma_e \sinh(\gamma_e h)} \tag{33}$$

$$Y_{\text{Transf.}}^{h} = \frac{\gamma_h}{\gamma_h \cosh(\gamma_h h) + \gamma_0 \sinh(\gamma_h h)}. \tag{34}$$

The reflected and transmitted fields in the top and bottom regions of the FSS structure are given, respectively, by

$$\begin{bmatrix} \tilde{E}_x^r \\ \tilde{E}_y^r \end{bmatrix} = j \frac{\gamma_0^2 - \gamma_h^2}{\gamma_0^2 + 2\gamma_0\gamma_h \coth(\gamma_h h) + \gamma_h^2} \begin{bmatrix} -\beta_0 \\ \alpha_0 \end{bmatrix} \tag{35}$$

$$\begin{bmatrix} \tilde{E}_x^t \\ \tilde{E}_y^t \end{bmatrix} = j \frac{\frac{2\gamma_0\gamma_h}{\sinh(\gamma_h h)}}{\gamma_0^2 + 2\gamma_0\gamma_h \coth(\gamma_h h) + \gamma_h^2} \begin{bmatrix} -\beta_0 \\ \alpha_0 \end{bmatrix} \tag{36}$$

for TE modes, and as

$$\begin{bmatrix} \tilde{E}_x^r \\ \tilde{E}_y^r \end{bmatrix} = \frac{\gamma_0}{\omega\epsilon_0} \frac{\gamma_0^2\epsilon_{xx}^2 - \gamma_e^2}{\gamma_e^2 + 2\gamma_0\gamma_e\epsilon_{xx} \coth(\gamma_e h) + \gamma_0^2\epsilon_{xx}} \begin{bmatrix} \alpha_0 \\ \beta_0 \end{bmatrix} \tag{37}$$

$$\begin{bmatrix} \tilde{E}_x^t \\ \tilde{E}_y^t \end{bmatrix} = \frac{\gamma_0}{\omega\epsilon_0} \frac{\frac{2\gamma_0\epsilon_{xx}\gamma_e}{\sinh(\gamma_e h)}}{\gamma_e^2 + 2\gamma_0\gamma e\epsilon_{xx} \coth(\gamma_e h) + \gamma_0^2\epsilon_{xx}} \begin{bmatrix} \alpha_0 \\ \beta_0 \end{bmatrix} \tag{38}$$

for TM modes.

Substituting (35)–(38) into (24)–(27), the reflection and transmission coefficients for the FSS structure are determined.

III. Numerical Results

In this section, we present some numerical and experimental results to illustrate the application of techniques discussed previously in order to obtain reflection and transmission characteristics of FSS structures. Results obtained in this study were compared to results presented by Gross [7] and to measurement data,

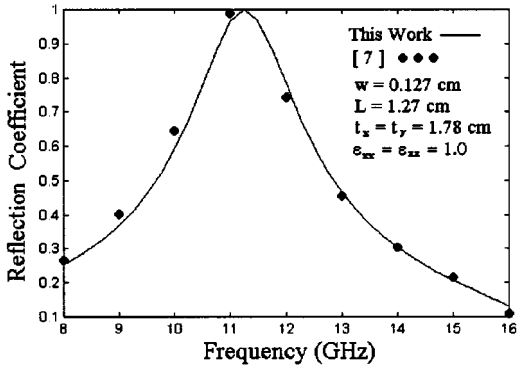

Fig. 3. Frequency behavior of the reflection coefficient from a freestanding FSS with rectangular conducting patches.

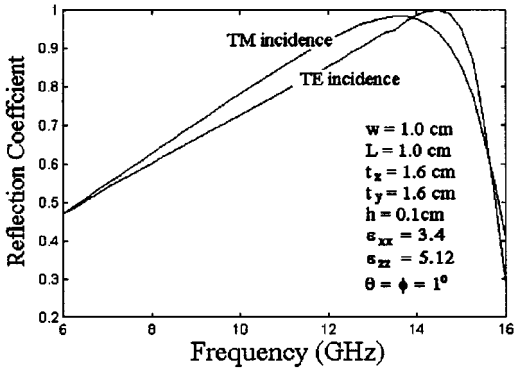

Fig. 6. Reflection coefficient from an FSS structure on an anisotropic dielectric layer for TE and TM incident modes.

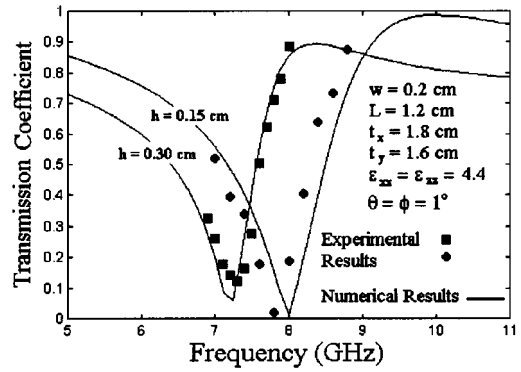

Fig. 4. Numerical results for an FSS structure with rectangular patches on a dielectric anisotropic substrate compared with experimental data.

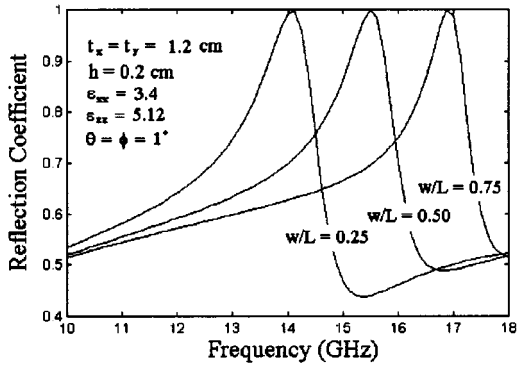

Fig. 5. Reflection coefficient from an FSS structure on a dielectric layer for different values of the patch aspect ratio W/L.

shown in Figs. 3 and 4, respectively. Curves for the reflection coefficient versus frequency on FSS structures with anisotropic substrate materials are shown in Figs. 5 and 6.

The first comparison analysis was performed for the case shown in Fig. 3 where a freestanding FSS was considered ($\epsilon_{xx} = \epsilon_{zz} = 1$) for a TEM incident mode and a plane wave normally incident ($\theta = \phi = 1°$). The reflection is seen to peak around 11 GHz. As can be seen, a very good agreement was obtained between these results.

The second comparison analysis was performed for the case shown in Fig. 4 between numerical and experimental results for an FSS structure on a dielectric layer. In this case, an FSS structure with rectangular conducting patches on an isotropic dielectric substrate was considered. The substrate material used in the implementation of the prototypes was Fiberglass ($\epsilon_{xx} = \epsilon_{zz} = 4.4$). A TE incident mode and a plane wave normally incident ($\theta = \phi = 1°$) were considered. The total reflection occurs around 8 GHz for $h = 0.15$ cm, and 7.2 GHz for $h = 0.3$ cm. As can be seen, a very good agreement was obtained between numerical and measured results.

Fig. 5 shows the reflection coefficient versus frequency for various values of the patch aspect ratio W/L, where W and L are, respectively, the patch width and length. The substrate material considered in this analysis was the pyrolytic boron nitride (PBN). As expected, the resonant frequency and bandwidth increases when the aspect ratio W/L increases.

Fig. 6 shows curves of the reflection coefficient for TE and TM incidences. For TE incidence, the resonance occurs at $f = 14.6$ GHz and the bandwidth is 5.93 GHz. For TM incidence, the resonance occurs at $f = 13.3$ GHz and the bandwidth is 6.79 GHz.

IV. Conclusions

The scattering of electromagnetic waves from FSS structures with rectangular conducting patches printed on a dielectric anisotropic substrate has been investigated in the spectral domain to determine reflection and transmission characteristics. Numerical results have been obtained as a function of the structural parameters. It has been observed that the use of anisotropic substrates increases the flexibility in the design of FSS structures on dielectric layers.

References

[1] R. Mittra, C. H. Chan, and T. Cwik, "Techniques for analyzing frequency selective surfaces: A review," *Proc. IEEE*, vol. 76, pp. 1593–1616, Dec. 1988.

[2] T. K. Wu, *Frequency Selective Surfaces and Grid Arrays*. New York: Wiley, 1995.

[3] T. K. Chang, R. J. Langley, and E. A. Parker, "Frequency selective surfaces on biased ferrite substrates," *Electron. Lett.*, vol. 30, no. 15, pp. 1193–1194, 1994.

[4] A. C. C. Lima, E. A. Parker, and R. J. Langley, "Tunable frequency selective surfaces using liquid substrates," *Electron. Lett.*, vol. 30, no. 4, pp. 281–282, 1994.

[5] N. V. Schuley, "Diode loaded frequency selective surfaces," in *Proc. JINA'92*, France, pp. 313–316.
[6] A. L. P. S. Campos, M. A. B. de Melo, and A. G. d'Assunção, "Frequency-selective surfaces with rectangular apertures on uniaxial anisotropic substrates," *Microwave Opt. Technol. Lett.*, vol. 25, no. 2, pp. 126–129, 2000.
[7] F. B. Gross, "Reflection from an array of conducting plates using classic edge-mode current densities," *IEEE Trans. Antennas Propagat.*, vol. 43, pp. 1333–1335, Nov. 1995.
[8] A. L. P. S. Campos, "Superfícies seletivas de freqüência sobre substratos dielétricos anisotrópicos uniaxiais," M.S. thesis (in Portuguese), Univ. Federal do Rio Grande do Norte, Natal RN, Brazil, 1999.
[9] T. Itoh, "Spectral domain immitance approach for dispersion characteristics of generalized printed transmission lines," *IEEE Trans. Microwave Theory Tech.*, vol. MTT-28, pp. 733–736, MONTH 1980.

Antonio Luiz P. S. Campos (S'01) received the B.S.E.E. and M.S.E.E. degrees from the Federal University of Rio Grande do Norte, Natal RN, Brazil, in 1996 and 1999, respectively, and is currently working toward the Ph.D. degree at the Federal University of Paraíba, Campina Grande PB, Brazil.

He is currently involved in the areas of FSS, scattering of electromagnetic waves, antennas, and planar devices.

He is a member of the IEEE Antennas and Propagation Society (IEEE AP-S) and the Brazilian Microwave and Optoelectronics Society (SBMO).

Adaildo Gomes d'Assunção (S'80–M'81) received the B.S.E.E. degree (with honors) from the Federal University of Rio Grande do Norte, Norte RN, Brazil, in 1974, and the M.S. and Doctoral degrees in electrical engineering from the State University of Campinas, Campinas SP, Brazil, in 1977 and 1981, respectively.

From 1975 to 1976, he was involved with radar and telemetry systems at the Launching Center of Barreira do Inferno, Natal RN, Brazil. Since 1976, he has been with the Federal University of Rio Grande do Norte, Natal RN, Brazil, where he is currently a Professor of electrical and electronics engineering. From 1985 to 1987, he was a Post-Doctoral Visiting Scientist with the Department of Electrical and Electronics Engineering, North Dakota State University, Fargo. He currently teaches and conducts research on antennas, microwave integrated circuits, millimeter waves, and optical communications.

Dr. d'Assunção is a member of the Brazilian Microwave and Optoelectronics Society (SBMO), the IEEE Microwave Theory and Techniques Society (IEEE MTT-S), and the IEEE Antennas and Propagation Society (IEEE AP-S).

Laércio Martins de Mendonça received the B.S.E.E. and M.S.E.E. degrees from the Federal University of Rio Grande do Norte, Natal RN, Brazil, in 1977 and 1987, respectively, and the Doctoral degree from the Federal University of Paraíba, Campina Grande PB, Brazil, in 1994.

In 1993, he joined the Federal University of Rio Grande do Norte, where he is currently an Associate Professor. His research activities are in microwave integrated circuits, millimeter waves, nonplanar transmission lines, and antennas.

Dr. Mendonça is a member of the Brazilian Microwave and Optoelectronics Society (SBMO) and the Brazilian Telecommunications Society (SBrT).